Accepted Manuscript

Title: Dielectric and electrical studies of Pr^{3+} doped nano $CaSiO_3$ perovskite ceramics

Author: Sandhya Kulkarni B.M. Nagabhushana Narsimha Parvatikar Anilkumar Koppalkar<ce:author id="aut0025" orcid="0000-0001-5655-019X"> C. Shivakumara R. Damle

PII: S0025-5408(13)00860-X
DOI: http://dx.doi.org/doi:10.1016/j.materresbull.2013.10.029
Reference: MRB 7110

To appear in: *MRB*

Received date: 30-10-2012
Revised date: 6-10-2013
Accepted date: 13-10-2013

Please cite this article as: S. Kulkarni, B.M. Nagabhushana, N. Parvatikar, A. Koppalkar, C. Shivakumara, R. Damle, Dielectric and electrical studies of Pr^{3+} doped nano $CaSiO_3$ perovskite ceramics, *Materials Research Bulletin* (2013), http://dx.doi.org/10.1016/j.materresbull.2013.10.029

Dielectric and electrical studies of Pr^{3+} doped nano $CaSiO_3$ perovskite ceramics

Sandhya Kulkarni[a*], B.M. Nagabhushana[b], Narsimha Parvatikar[c], Anilkumar Koppalkar[d], C. Shivakumara[e] and R. Damle[a]

[a] Department of Physics, Bangalore University, Bangalore-560 056, India.
[b] Department of Chemistry, M.S. Ramaiah Institute of Technology, Bangalore-560 054, India.
[c] Department of Physics, APS College of Engineering, Bangalore-560 082, India.
[d] Department of Physics, S. S. Margol College, Shahabad-585 228, India.
[e] Department of Solid State and Structural Chemistry Unit, Indian Institute of Science, Bangalore-560 012, India.

Abstract

$CaSiO_3$ nano ceramic powder doped with Pr^{3+} has been prepared by solution combustion method. The powder $Ca_{0.95}Pr_{0.05}SiO_3$ is investigated for its dielectric and electrical properties at room temperature to study the effect of doping. The sample is characterized by X-ray diffraction and Infrared spectroscopy. The size of either of volume elements of $CaSiO_3$:Pr^{3+} estimated from Transmission electron microscopy is about 180-200nm. The sample shows colossal dielectric response at room temperature. This colossal dielectric behaviour follows Debye type relaxation and can be explained by Maxwell-Wagner polarization. However, analysis of impedance and electric modulus data using Cole-Cole plot shows that it deviates from ideal Debye behaviour resulting from the distribution of relaxation times. The distribution in the relaxation times may be attributed to existence of electrically heterogeneous grains, insulating grain boundary and electrode contact regions. Doping thus results in substantial modifications in the dielectric and electrical properties of the nano ceramic $CaSiO_3$.

Keywords. Nanoceramics; perovskites; dielectric properties; electric modulus; ac conductivity.

---

*Corresponding Author: Sandhya Kulkarni, Email ID: pappu.sandhyakulkarni@gmail.com
Tel.:+919243017429

1. Introduction

Perovskite ceramics are widely used in various electronics and microelectronic devices. Traditionally, ferroelectric materials are used for the purpose of reduction in the size of capacitive components, offering an opportunity to miniaturize electronic systems. However, use of ferroelectrics is limited by the strong temperature dependence of dielectric constant near transition temperature T_C. In the recent years, a large number of non-ferroelectric materials such as $CaCu_3Ti_4O_{12}$ (CCTO) [1-3], $BaFe_{1/2}Nb_{1/2}O_3$ [4], $LaFeO_3$ [5] and $Pr_{0.6}Ca_{0.4}MnO_3$ [6] have been found to possess colossal values of the dielectric constant with a weak temperature dependence. Tsang-Tse Fang et al. have investigated the role of Si ions in the microstructure change, the electrical conduction and the dielectric responses of $CaSiO_3$ doped CCTO [7].

It has been accepted that the large dielectric constant at room temperature, possessed by CCTO ceramic perovskites, is due to the Maxwell-Wagner contributions of depletion layer at grain boundaries or interfaces between the sample and contacts. This electrical microstructure reflects the microstructure of an internal barrier layer capacitor (IBLC), which acts as a passive element in the miniaturised electronic circuits. Grains, especially at grain surfaces, may show small variations in composition upon doping. Such variations are responsible for the characteristic properties of varistors and barrier layer capacitors. Impedance spectroscopy can reveal such compositional variations while it may be difficult to detect such compositional variations by electron microscopy.

N Tangboriboon et al have prepared $CaSiO_3$ using eggshell and fumed silica by Sol-gel method and have observed high dielectric constant [8], whereas a different value of dielectric constant was observed for nano $CaSiO_3$, prepared by solution combustion process in our previous work [9].

In this work, we have examined the dielectric and electrical properties of Pr doped nano $CaSiO_3$ ceramic to investigate the changes in dielectric and electrical properties upon doping.

2. Experimental

5 mole % of Pr_2O_3 was first converted into the corresponding nitrate by dissolution in 1:1 dilute nitric (HNO_3). The product is then added to stoichiometric quantities of analar grade calcium nitrate ($Ca(NO_3)_2\ 4H_2O$), fumed silica (SiO_2 of 99.9% purity and surface area of 200 m^2/gm) and citric acid ($C_6H_8O_7$) (which acts as a fuel for redox reaction) in a minimum quantity of water and dispersed well using magnetic stirrer for half an hour. The heterogeneous redox mixture was then rapidly heated in a muffle furnace maintained at 500 ± 10 °C. The redox mixture when heated at 500 °C boils, thermally dehydrates and ignites to yield fluffy, porous $Ca_{0.95}Pr_{0.05}SiO_3$ powder.

The stoichiometry of the redox mixture used for combustion process was calculated using total oxidizing and reducing valencies of the ingredients which serve as numerical coefficients for the stoichiometric balance so that the equivalence ratio (ϕ_c) is unity and the energy released by the combustion is maximum [10].

The powder was then sintered at 900 °C for three hours in order to attain a single phase. This powder was pressed (without the addition of any binder) into pellets for measurements. The pellets were coated with silver paste for better electrical contact. The dielectric measurements were carried out at room temperature using Hioki impedance analyzer 3532-50 (Japan) in the frequency range 10^2 - 10^6 Hz at 2mV applied potential. Complex impedance, electric modulus and ac conductivity are estimated from the dielectric measurement data.

The determination of inter-planar spacing, lattice parameters and *hkl* values etc. provide a basis for the understanding of the structure of the solids. In the present work, to characterize the powder, a powder X-ray diffractometer (Phillips X'pert) using CuK_α radiation (λ = 0.15405 nm) with a Ni-filter was used to record the powder diffractograms. The size distribution of the grains was examined by Transmission Electron Microscopy (TEM). A JEM 2000 Ex instrument was used to record TEM micrographs. Fourier Transform Infrared (FTIR) spectroscopy was used to study the effect of doping on the vibratonal bands of $CaSiO_3$. An Alpha Bruker FTIR spectrometer has been used to record the IR spectra of the investigated ceramic powders.

3. Results and Discussion

For ABO_3 ionic solids, the degree of distortion is described by the tolerance factor,

$$t = \frac{(r_A + r_O)}{\sqrt{2}(r_B + r_O)} \quad (1)$$

where r_A , r_B and r_O represent ionic radii of A, B and oxygen ions respectively. The ideal cubic perovskite $SrTiO_3$ has a tolerance factor (t) equal to unity. For distorted cubic structures, the value of t will be less than or greater than 1. Since $CaSiO_3$ has 'distorted cubic' (monoclinic) structure, we get t = 0.673 for r_{Ca} = 0.099 nm, r_O = 0.126 nm and r_{Si} = 0.111 nm. The substitution of Pr^{3+} in the Ca^{2+}site does not change the value of tolerance factor, as the ionic radius of Pr^{3+} is same (0.099 nm) as that of Ca^{2+}. The sintering aid is not required for ceramic materials having the value of tolerance factor $t < 0.98$, as observed by Abdul Khalam et al. [11]. However, when Pr^{3+} ions are substituted in the A-site (Ca^{2+}-site), cation vacancies are produced in the perovskite structure. Obviously, the number of vacancies increases with increasing Pr^{3+} content. Pr exists in tri and tetra-oxidation states. Tri-oxidation

state is more stable than tetra-oxidation state. Hence Pr occupancy in B-site is unlikely and thus it replaces Ca^{2+} ions in the A-site. This substitution could reduce the oxygen vacancies by forming A-site vacancy and oxygen vacancy defect dipoles. This would increase electric displacements thus increasing the dielectric constant.

3.1 Powder X-Ray Diffraction (XRD) results

The phase evaluation of the solution combustion derived products was examined by powder X-ray diffraction. The as-formed undoped and Pr^{3+} doped $CaSiO_3$ products were amorphous in nature, so they were calcined at 900°C for 3 hrs to get crystalline and phase pure products. The powder XRD patterns of thus calcined undoped and Pr^{3+} doped samples are shown in Figure 1. The undoped sample shows pure β phase with no other impurity peaks, whereas doped sample shows mainly β phase but with small number of α peaks. All the diffraction peaks match very well with the standard values from the Joint Committee on Powder Diffraction Standards (JCPDS) (data card No. 84-0655) which were readily indexed to monoclinic phase with space group $P2_1/a$.

3.2 Transmission Electron Microscopy (TEM) results

In the TEM image of $Ca_{0.95}Pr_{0.05}SiO_3$ shown in Figure 2, the particles have been observed to be agglomerated, forming two volume elements of the sample. The size of either of these elements has been approximated to be in the range of 180-200 nm.

3.3 Fourier Transform Infra Red (FTIR) Spectroscopy results

The FTIR spectra of undoped $CaSiO_3$ and Pr^{3+} doped $CaSiO_3$ powders have been recorded to provide information on their structures (Figure 3). Both the samples show IR peaks at 471, 508, 665,680, 904 and 964 cm^{-1} are attributed to the β –$CaSiO_3$. The absorption bands occurring around 415-600 cm^{-1} are due to Si-O stretching vibration and absorption bands in the range 750-1170 cm^{-1} are due to O-Si-O stretching vibration [12]. However the absorption

bands of Si-O vibration as well as those of O-Si-O vibration are observed to be more stretched in the Pr doped $CaSiO_3$ spectra leading to the stress created on the bonds by A-site cation vacancies resulting from Pr^{3+} substitution in Ca^{2+} site.

3.4 Dielectric Studies

The frequency dependence of the dielectric constant and dielectric loss tangent for undoped nano $CaSiO_3$ at room temperature is shown in Figure 4. A normal relaxation was observed in undoped nano $CaSiO_3$ ceramic prepared by solution combustion method and no relaxation peak was observed in loss tangent plot versus frequency [9]. Thus the electrical microstructure of undoped nano $CaSiO_3$ is homogeneous and hence its dielectric behaviour does not follow the Maxwell Wagner (MW) relaxation.

The variation of dielectric constant and dielectric loss tangent with frequency for $Ca0_{.95}Pr_{0.05}SiO_3$ ceramic is shown in the Figure 5. The dielectric constant of the sample decreases from a high value of about $7.5x10^5$ to a value of about 4000 as the frequency is varied from 100 Hz to 6 KHz. The high dielectric constant at lower frequencies (below 500 KHz) may be attributed to the presence of space charge produced due to electrode-sample contact and interface between the grains and their boundaries. The dielectric behaviour of $Ca_{0.95}Pr_{0.05}SiO_3$ ceramic has a Debye-like relaxation with a steep decrease in dielectric constant at the frequency where the loss tangent plot versus frequency displays a relaxation peak. The Debye-like relaxation can be explained by MW polarization. The value of loss tangent has been increased at lower frequencies in Pr^{3+} doped sample compared to that of undoped sample, as the cation vacancies are produced by substituting Pr^{3+} ions in Ca^{2+} sites, in the doped sample.

MW polarization arises as a result of different extrinsic effects resulting in the heterogeneities in the system. One common effect is the electrode-sample contact, where a

barrier layer with high capacitance in parallel with a large resistance is formed. Heterogeneities in the system, i.e., grain-grain contacts (grain boundaries) may also contribute to this [13, 14]. This high capacitance results in a high dielectric constant.

3.5 Impedance Spectroscopy

Complex impedance spectroscopy is a non-destructive testing technique for analysing the electrical processes in a compound on the application of an AC signal as input perturbation. We have used Impedance Spectroscopy (IS) to establish the electrical microstructure of $Ca_{0.95}Pr_{0.05}SiO_3$ ceramics. The impedance response of a polycrystalline compound (when plotted in a complex plane) reveals the contribution from grain, grain boundary and electrode properties with different time constants leading to successive semicircles. IS can be useful to study the relaxation processes during the charge transport within the electronic ceramics [4]. In most types of the electronic ceramics, the relaxations are non-uniform which show distribution of relaxation times, so that a Cole-Cole type distribution prevails.

The real (Z′) and imaginary (Z″) parts of the impedance are evaluated from dielectric measurements using the identities $Z' = \text{Mod } Z\ (\text{Cos}\Phi)$ and $Z'' = \text{Mod } Z\ (\text{Sin}\Phi)$ and complex impedance plots are obtained. Figure 6 exhibits the complex impedance plot.

In ceramics with conducting grains, grains are less resistive than grain boundaries and the electrode contacts. In other words the resistance and the capacitance of the electrode-sample contact and grain boundaries are always larger than those of the bulk grains. This effect may be explained on the basis of non-stoichiometric distribution of oxygen and the presence of dangling bonds on the grain boundaries and grain electrode contact, which act as carrier traps. This results in the formation of a barrier layer known as Schottky barrier for the carrier transport. This thin layer of relatively large resistance offers higher capacitance owing to the inverse proportionality between the capacitance C and thickness d of the layer. This high

resistance and capacitance associated with the grain electrode contact and grain boundaries cause their response to lie at lower frequencies compared to that of grains [5].

If R_{ge}, R_{gb}, R_g and C_{ge}, C_{gb}, C_g denote the resistances and capacitances associated with grain electrode contact, grain boundaries and grain interiors respectively, then the impedance at room temperature associated with the equivalent circuit in the inset of the figure 6 is given by Debye equation

$$Z^* = Z' - jZ'' \tag{2}$$

where

$$Z' = \left[\frac{R_{ge}}{1+(\omega R_{ge}C_{ge})^2} + \frac{R_{gb}}{1+(\omega R_{gb}C_{gb})^2} + \frac{R_g}{1+(\omega R_g C_g)^2}\right] \tag{3}$$

and

$$Z'' = \left[\frac{\omega {R_{ge}}^2 C_{ge}}{1+(\omega R_{ge}C_{ge})^2} + \frac{\omega {R_{gb}}^2 C_{ge}}{1+(\omega R_{gb}C_{gb})^2} + \frac{\omega {R_g}^2 C_g}{1+(\omega R_g C_g)^2}\right] \tag{4}$$

The impedance response then may be described by the Cole-Cole equation rather than the ideal Debye equation. It is given by

$$Z^*(\omega) = \frac{R}{1+\left(\frac{j\omega}{\omega_0}\right)^{1-\alpha}} \tag{5}$$

When α goes to zero, the equation (5) leads to the classical Debye behaviour. The exponent 'α' represents the magnitude of the departure of the electrical response from an ideal condition having a single relaxation time. In other words, 'α' represents the distribution of relaxation times [15]. Considering the experimental features, the existence of the distribution of relaxation times is correlated to some semicircle depression degree. The magnitude of the depression is given by decentralization angle (β), which can be derived from the equation

$$\propto = {}^{2\beta}/_{\pi} \qquad (6)$$

The Cole-Cole fit has been fitted for portion (a) of the plot in figure 6. A nonlinear fit using ORIGIN software is shown in the figure 7. The fit **has been** found to have a convergence of 0.95. The fit parameters are the coordinates of the centre of the semicircle (x_o, y_o) and its radius r which have been obtained as follows.

x_o = 2303.25 units, y_o = - 2542.74 units and r = 3937.16 units.

For an exact semicircle the centre lies on the positive X-axis, that represents ideal Debye relaxation. In this case x_0 is positive and y_0 is negative showing that the dielectric behaviour of the sample is non-Debye type. The deviation from Debye relaxation is thus identified from the position of the centre of the semicircle.

The exponent α in this model is given by the equation

$$\left(\frac{z_0 - z_\infty}{2}\right) tan\left(\frac{\alpha\pi}{2}\right) = y_0 \qquad (7)$$

where

$$\left(\frac{z_0 - z_\infty}{2}\right) = x_0$$

The estimated value of α is equal to 0.53. The value of β calculated using the equation (6), is found to be equal to 0.83. This clearly reflects distribution of relaxation times in our system. The error bars in the fit represent the deviation of experimental data from the fitted values. The phenomenon of distribution in relaxation times ($\alpha < 1$) has been reported earlier for ceramics with perovskite structures [16, 17]. Nobre et al. reported that there is a distribution of relaxation times for $\beta < 1.57$ [15]. Thus the Cole-Cole fit shows a broad distribution of relaxation times due to both grain and grain boundaries and the part (b) (a tail like structure) in figure 6 represents the grain electrode contact contribution.

As a first approximation, these complex impedance plots (Nyquist plot) can be represented by the equivalent circuit models shown in the inset of the figure 6. Each contribution is represented by a parallel resistance-capacitance equivalent circuit corresponding to the individual component of the material i.e., grain, grain boundary and grain electrode contact respectively, from higher to lower frequency values in the anticlockwise direction.

The figure 8 describes that, the magnitude of Z′ decreases with increase in frequency indicating an increase in ac conductivity. A Debye like peak in the frequency dependence of the Z" in the same figure usually indicates the presence of space charges [18].

3.6 Conductivity formalism

The variation of ac conductivity versus frequency for undoped and Pr doped $CaSiO_3$ is shown in figure 9. The conductivity of the system increases by orders of magnitude upon doping. A convenient formalism to investigate the frequency behaviour of conductivity at room temperature is based on the power law proposed by Jonscher.

$$\sigma(\omega) = \sigma(0) + A\omega^n \qquad (8)$$

where σ(ω) is the total conductivity, σ(0) is the frequency independent conductivity (dc conductivity), A is a constant which determines the strength of polarizability and 'n' is the

power law exponent that represents the degree of interaction between the mobile ions with the lattice around them. Jonscher has shown that a nonzero 'n' value in the dispersive region of conductivity is due to the energy stored in the short range collective motion of ions. A higher value of 'n' implies that large energy is stored in such collective motions [19]. The value of n is 0.90 for un-doped sample [9]. With doping, the conductivity is found to increase as the grain resistance dominates over grain boundary resistance, and the value of n increases to 0.92.

In a hopping model, it is possible to distinguish different characteristic regions of frequency. At low frequencies where conductivity is constant, carrier transport takes place in its finite paths due to non-localized carriers. In the region of frequencies where conductivity increases markedly with frequency, the carriers can hop only between two sites and a total response is produced by the sum of the individual responses of pairs of sites randomly distributed throughout the material due to localized carriers [20].

3.7 Electric modulus formalism

The electrical modulus is the reciprocal of the permittivity

$$M^* = 1/\varepsilon^* \tag{9}$$

For a dielectric relaxation process, a relaxation peak appears in both M^* and ε^* representation. Comparisons of the ε^* and M^* representations have been used to distinguish localized dielectric relaxation processes from long range conductivity. Physically, the electrical modulus corresponds to the relaxation of the electric field in the material when the electric displacement remains constant, so that the electric modulus represents the real dielectric

relaxation process, which can be expressed as

$$M^* = {}^{1}/_{\varepsilon^*} = M' + jM''$$

$$= M_\infty \left[1 - \int_0^\infty \left({}^{d\emptyset(t)}/_{dt}\right) exp(-i\omega t) dt\right] \quad (10)$$

where $$M_\infty = (\varepsilon_\infty)^{-1} \quad (11)$$

is the asymptotic value of M'(ω) and φ(t) is the time evolution of the electric field within the material [21]. M′ and M″ are evaluated from the dielectric measurements using the following identities

$$M' = {}^{\varepsilon'}/_{(\varepsilon'^2 + \varepsilon''^2)} \quad \text{and}$$

$$M'' = {}^{\varepsilon''}/_{(\varepsilon'^2 + \varepsilon''^2)} \quad (12)$$

M' and M" values can also be written in terms of resistance and capacitance as

$$M' = \frac{C_0}{C_{ge}}\left[\frac{(\omega R_{ge} C_{ge})^2}{1 + (\omega R_{ge} C_{ge})^2}\right] + \frac{C_0}{C_{gb}}\left[\frac{(\omega R_{gb} C_{gb})^2}{1 + (\omega R_{gb} C_{gb})^2}\right] + \frac{C_0}{C_g}\left[\frac{(\omega R_g C_g)^2}{1 + (\omega R_g C_g)^2}\right] \quad (13)$$

$$M'' = \frac{C_0}{C_{ge}}\left[\frac{\omega R_{ge} C_{ge}}{1 + (\omega R_{ge} C_{ge})^2}\right] + \frac{C_0}{C_{gb}}\left[\frac{\omega R_{gb} C_{gb}}{1 + (\omega R_{gb} C_{gb})^2}\right] + \frac{C_0}{C_g}\left[\frac{\omega R_g C_g}{1 + (\omega R_g C_g)^2}\right] \quad (14)$$

From equation (14), we can easily see that the response peaks of the grains, grain boundary and grain electrode contact effects occur in M" at frequencies,

$$\frac{1}{(2\pi R_{ge} C_{ge})}, \quad \frac{1}{(2\pi R_{gb} C_{gb})} \quad \text{and} \quad \frac{1}{(2\pi R_g C_g)}.$$

Since peak values are proportional to the reciprocals of the associated capacitances, the smaller capacitance should dominate in the electric modulus plots. The grains usually have smaller capacitance than the grain boundaries and hence their response peaks show up stronger in the modulus spectra [14]. The complex electric modulus spectrum (M′ versus M") is shown in the Figure 10. Here the single relaxation process due to grains is dominant over the contribution from grain boundaries and electrode-sample contact. The frequency dependence of M′(ω) and M"(ω) are shown in the figure 11. At lower frequencies, M′(ω) approaches to zero, confirming the presence of an appreciable ionic polarization at grain electrode contact and/or grain boundaries [22].

The frequency region below peak maximum in M"(ω) versus frequency determines the range in which charge carriers are mobile on long distances. At frequencies above peak maximum in M", the carriers are confined to potential wells, being mobile only at short distances [23].

Since the grains, grain boundaries and grain electrode contact are not really ideal RC elements, we observe that the shapes of the Z″ and M″ peaks are broader than the Debye peaks. This broadening of the response might be due to an inherently nonexponential processes such as correlation between diffusive motion of the ions or non-uniformities in the material microstructure. This leads in turn to a spatial distribution of local conductivities and electrical response times [14].

4. Conclusions

The colossal dielectric behaviour of Pr doped β-$CaSiO_3$ follows Debye type relaxation analysed by Maxwell-Wagner polarization. However, complex impedance and electric modulus when analysed by Cole-Cole plots indicate a non-Debye relaxation process which may be attributed to distribution in the relaxation times. A comparison of the conductivity and the imaginary part of electrical modulus suggests that both long range and localized

conduction are responsible for dielectric relaxation. The sample thus exhibits electrically inhomogeneous grains, grain boundary and electrode contact regions. This is the desired electrical microstructure analogous to CCTO for IBLCs. Thus doping of perovskite ceramics appears to substantially modify their dielectric and electrical properties as evident from the present investigations. Doping offers an efficient and useful tool to engineer nano ceramic materials with colossal dielectric constant for specific applications. It would be interesting to carry out the studies on the temperature dependence of dielectric and electrical response of the same.

Acknowledgments

Sandhya Kulkarni thanks the University Grants Commission (UGC), Government of India, for the award of UGC-FIP fellowship to carry out this work. She would also like to thank her fellow colleague Mr. Sriprakash G. for his valuable suggestions in plotting Cole-Cole fit.

References

[1] A.P. Ramirez, M.A. Subramanian, M. Gardel, G. Blumberg, D. Li, T. Vogt, S.M. Shapiro, Solid State Communications, 115 (2000) 217-220

[2] J. Li, A.W. Sleight, M.A. Subramanian, Solid State Communications 135 (2005) 260 – 262

[3] Laijun Liu, Huiqing Fan, Pinyang Fang, Li Jin, Solid State Communications 142 (2007) 573-576

[4] U. Intatha, S. Eitssayeam, J. Wang, T. Tunkasiri, Curr. Appl. Phys. 10 (2010) 21-25

[5] M. Idrees, M. Nadeem, M. Atif, M. Siddique, M. Mehmood, M.M. Hassan, Acta Materialia 59 (2011) 1338-1345

[6] N. Biskup, Andres A de, J.L. Martinez,Phys.Rev. B. 72 (2005) 024115

[7] Tsang-Tse Fang, Wei-Jie Lin, Chia-Ying Lin, Phys. Rev. B 76 (2007) 045115

[8] Nuchnapa Tangboriboon, Tunchanoke Khongnakhon, Supawinee Kittikul, Ruksapong Kunanuyuksapong, Anuvat Sirivat, J. Sol-Gel Sci. Technol., 58 (2011) 33-41

[9] Sandhya Kulkarni, B.M. Nagabhushana, Narsimha Parvatikar, C. Shivakumara, R. Damle, ISRN Material Science, 2011, ID 808560, (2011) 1-6
doi: 10.5402/2011/808560

[10] J.J. Kingsley, K.C. Patil, Mater. Lett. 6 (1988) 427-432

[11] L. Abdul Khalam, H. Sreemoolanathan, R. Ratheesh, P. Mohanan, M. T. Sebastian, Materi. Sci. Eng. B 107 (2004) 264-270

[12] R.P. Sreekanth Chakradhar, B.M. Nagabhushana, G.T. Chandrappa, K.P. Ramesha, J.L. Rao, Materi. Chem. and Phys. 95 (2006) 169–175

[13] P. Lunkenheimer, V. Bobnar, A. V. Pronin, A. I. Ritus, A. A. Volkov, A. Loidl, Phys. Rev.B 66 (2002) 052105

[14] J. Liu, C.G. Duan, W.G. Yin, W.N. Mei, R.W. Smith, J.R. Hardy, Phys. Rev. B. 70 (2004) 144106

[15] M.A.L. Nobre, S. Lanfredi, J. of Phys. and Chem. of Solids 64 (2003) 2457–2464

[16] M.A.L. Nobre, S. Lanfredi, J. Phys.: Condens. Matter 12 (2000) 7833–7841

[17] M.A.L. Nobre, S. Lanfredi, J. Phys. Chem. Solids 62 (2001) 1999–2006

[18] P.S. Sahoo, A. Panigrahi, S.K. Patri, R.N.P. Choudhary, Bull.Mater. Sci. 33 (2010) 129 -134

[19] Jonscher A K 1983 Dielectric relaxation in solids (London: Chelsea Dielectric Press)

[20] Pritam Kumar, B. P. Singh, T. P. Sinha, N. K. Singh, Adv. Mat. Lett. 3(2) (2012) 143-148

[21] Jianjun Liu, Chun-Gang Duan, Wei-Guo Yin, W. N. Mei, R. W. Smith, J. R. Hardy, J. Of Chem. Phys., 119(5) (2003) 2812-2819

[22] K. Srinivas, P. Sarah, S.V. Suryanarayana, Bull.Mater. Sci., 26 (2003) 247–253

[23] T. Badapanda, V. Senthil, S.K. Rout, L.S. Cavalcante, A.Z. Simoes, T.P. Sinha, S. Panigrahi, M.M. de Jesus, E. Longo, J.A. Varela,Current Appl.Phys.30 (2011) 1-12

Figure Captions

Figure 1 Powder XRD patterns of (a) undoped $CaSiO_3$ and (b) Pr doped $CaSiO_3$.

Figure 2 TEM image of Pr doped $CaSiO_3$ powder.

Figure 3 FTIR spectra of (a) undoped $CaSiO_3$ and (b) Pr doped $CaSiO_3$.

Figure 4 Dielectric constant and tanδ versus frequency for undoped $CaSiO_3$.

Figure 5 Dielectric constant and tanδ versus frequency for Pr doped $CaSiO_3$.

Figure 6 Complex impedance plane plot for Pr doped $CaSiO_3$ (Nyquist plot) with the inset showing the equivalent circuit.

Figure 7 Cole-Cole fit of Z'' versus Z' for Pr doped $CaSiO_3$.

Figure 8 Z' and Z" versus frequency for Pr doped $CaSiO_3$.

Figure 9 AC conductivity versus frequency for (a) undoped $CaSiO_3$ and (b) Pr doped $CaSiO_3$.

Figure 10 Complex electric modulus spectrum for Pr doped $CaSiO_3$.

Figure 11 M' versus and M" versus frequency for Pr doped $CaSiO_3$.

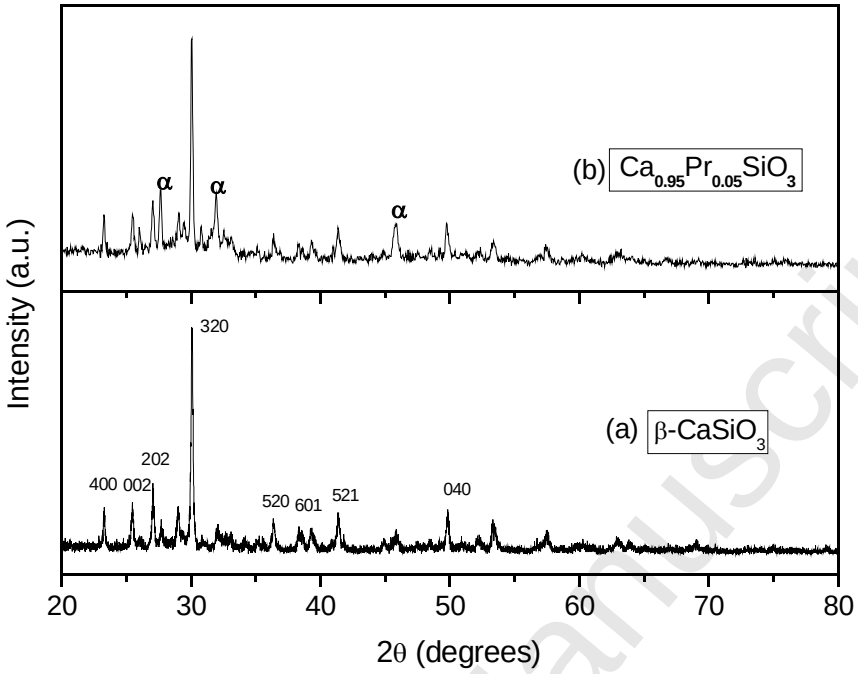

Figure 1 Powder XRD patterns of (a) undoped $CaSiO_3$ and (b) Pr doped $CaSiO_3$.

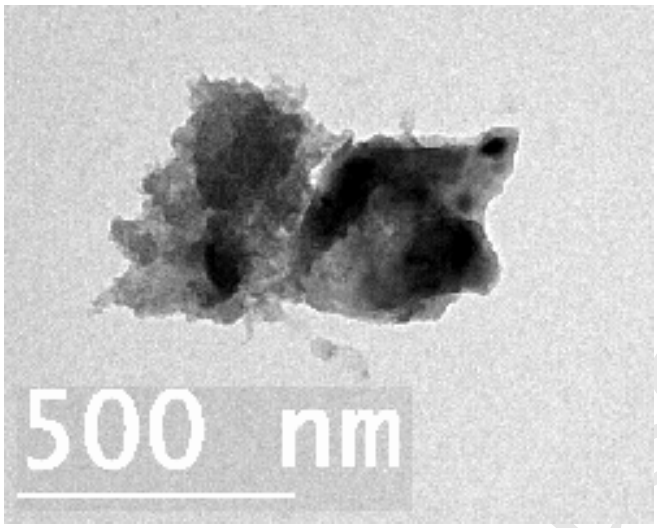

Figure 2 TEM image of Pr doped $CaSiO_3$ powder.

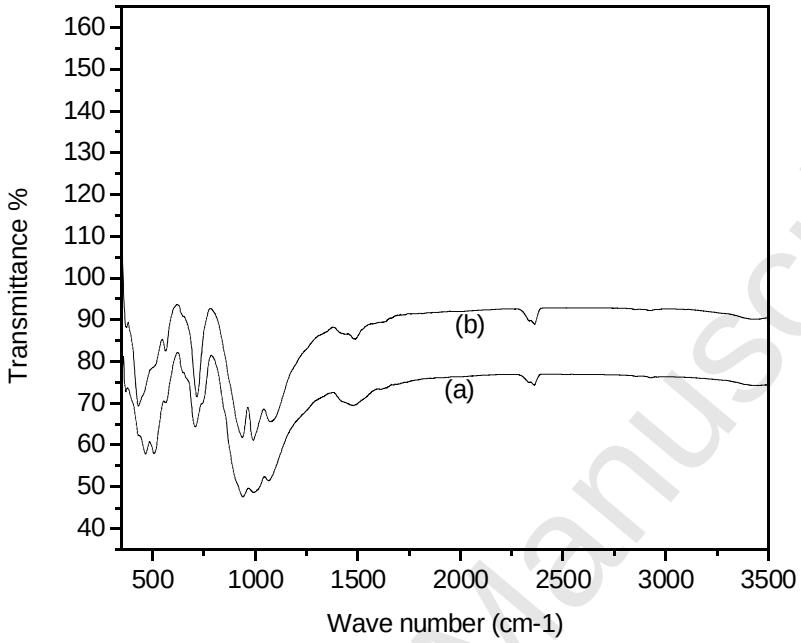

Figure 3 FTIR spectra of (a) undoped $CaSiO_3$ and (b) Pr doped $CaSiO_3$.

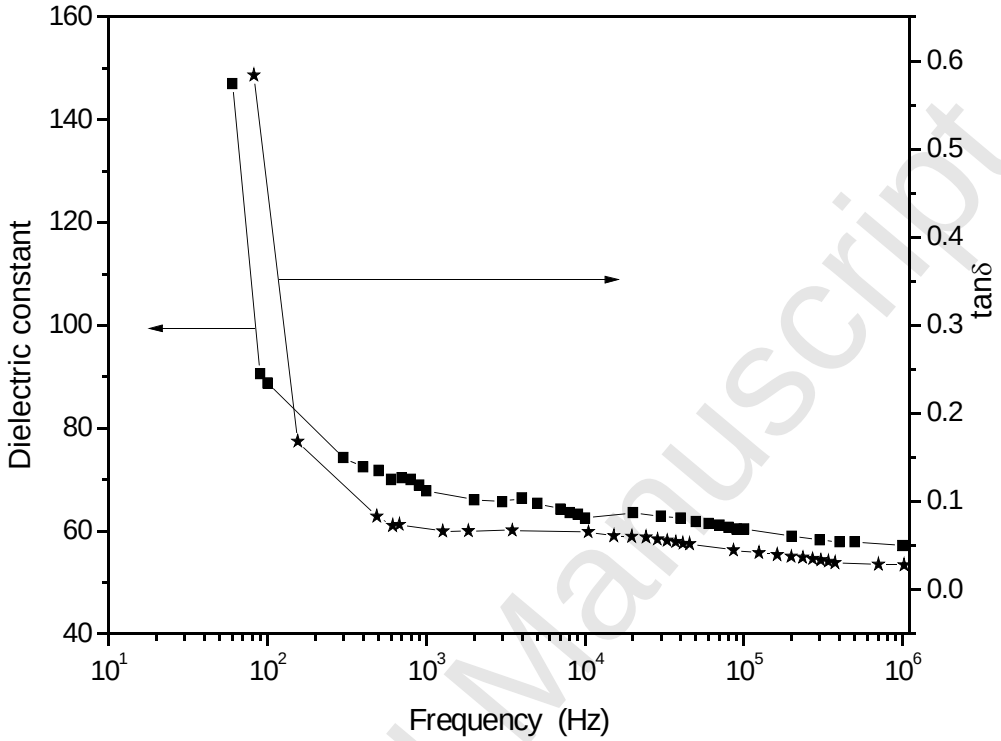

Figure 4 Dielectric constant and tanδ versus frequency for undoped $CaSiO_3$.

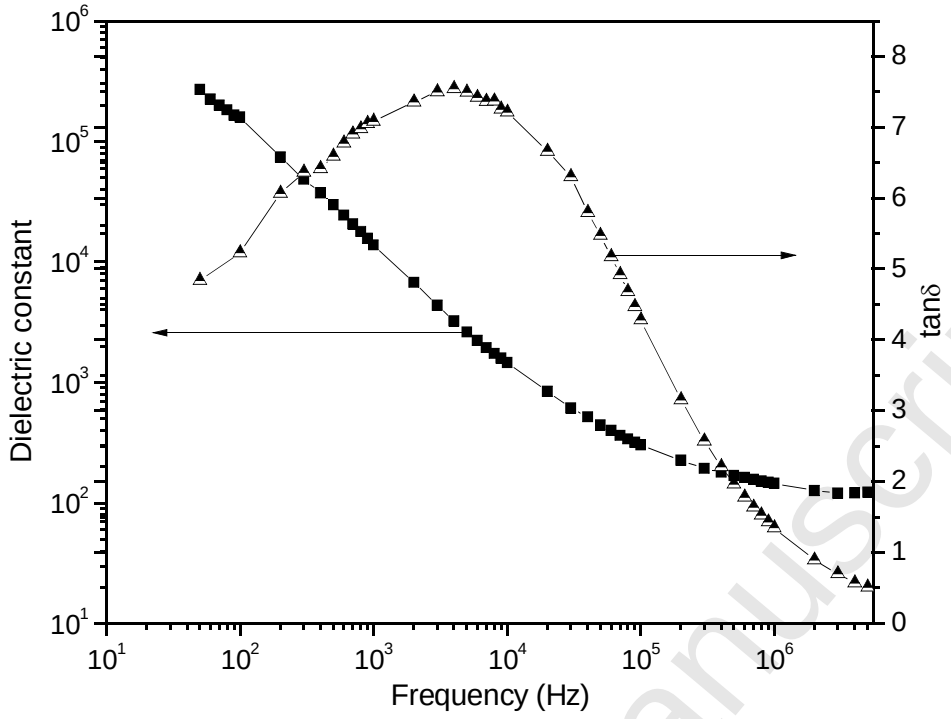

Figure 5 Dielectric constant and tanδ versus frequency for Pr doped $CaSiO_3$.

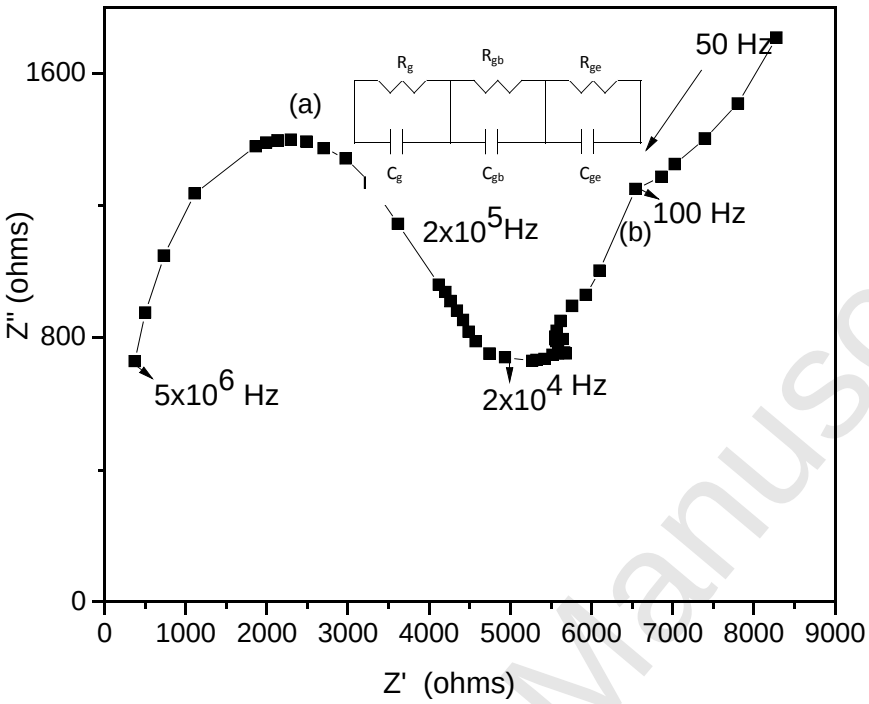

Figure 6 Complex impedance plane plot for Pr doped $CaSiO_3$ (Nyquist plot) with the inset showing the equivalent circuit.

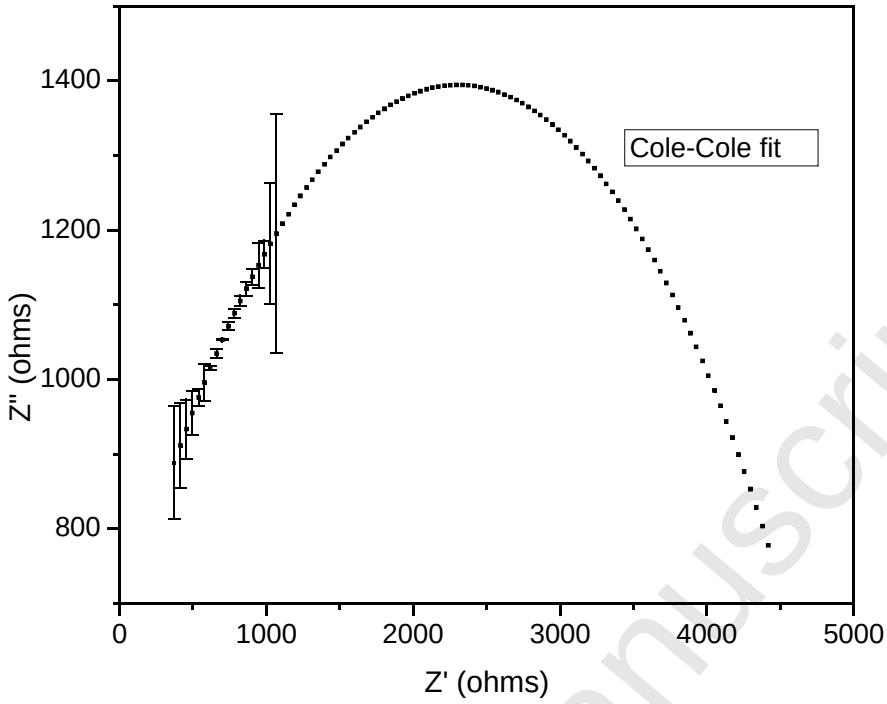

Figure 7 Cole-Cole fit of Z″ versus Z′ for Pr doped $CaSiO_3$.

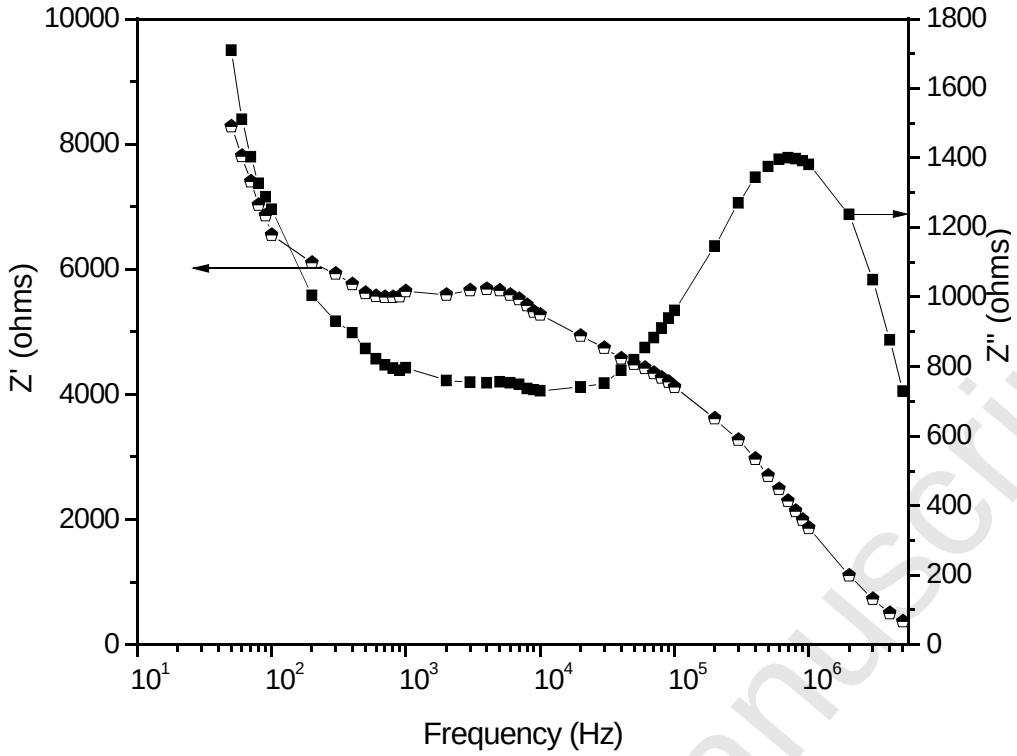

Figure 8 Z' and Z'' versus frequency for Pr doped $CaSiO_3$.

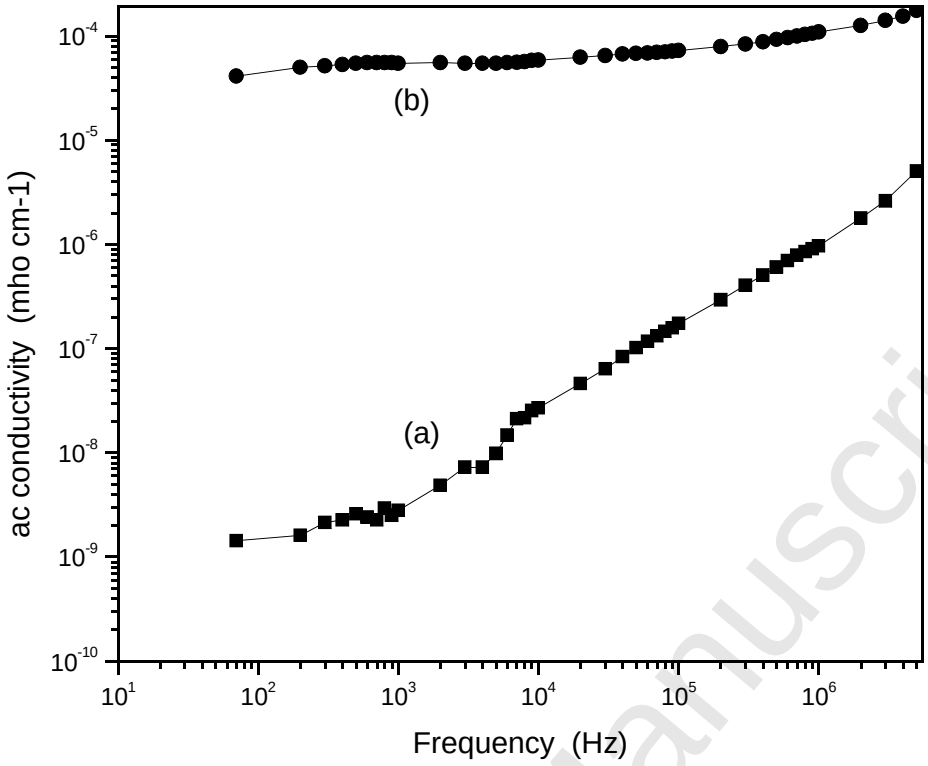

Figure 9 AC conductivity versus frequency for (a) undoped $CaSiO_3$ (b) Pr doped $CaSiO_3$.

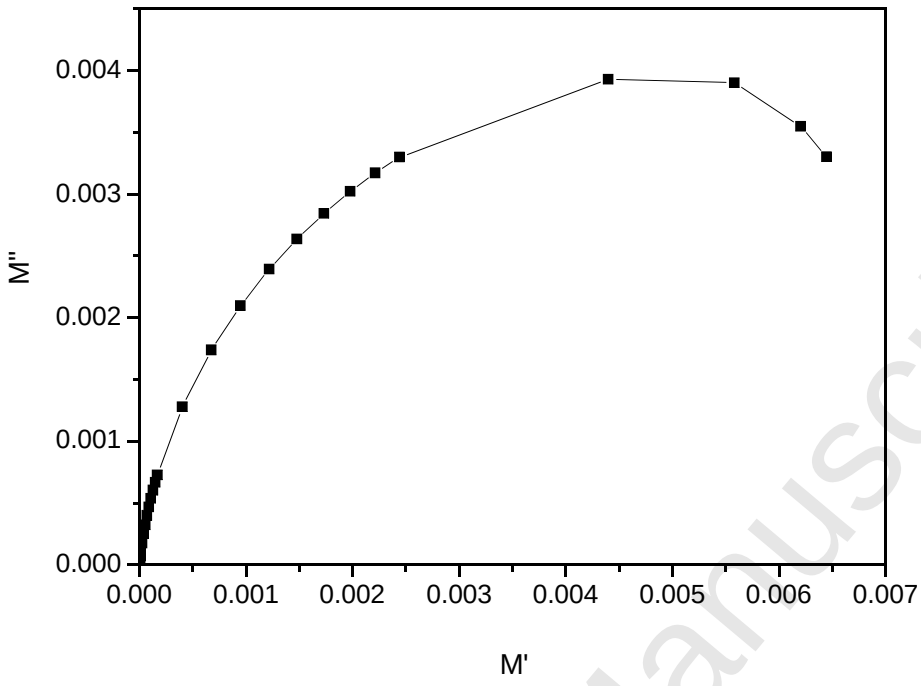

Figure 10 Complex electric modulus spectrum for Pr doped $CaSiO_3$.

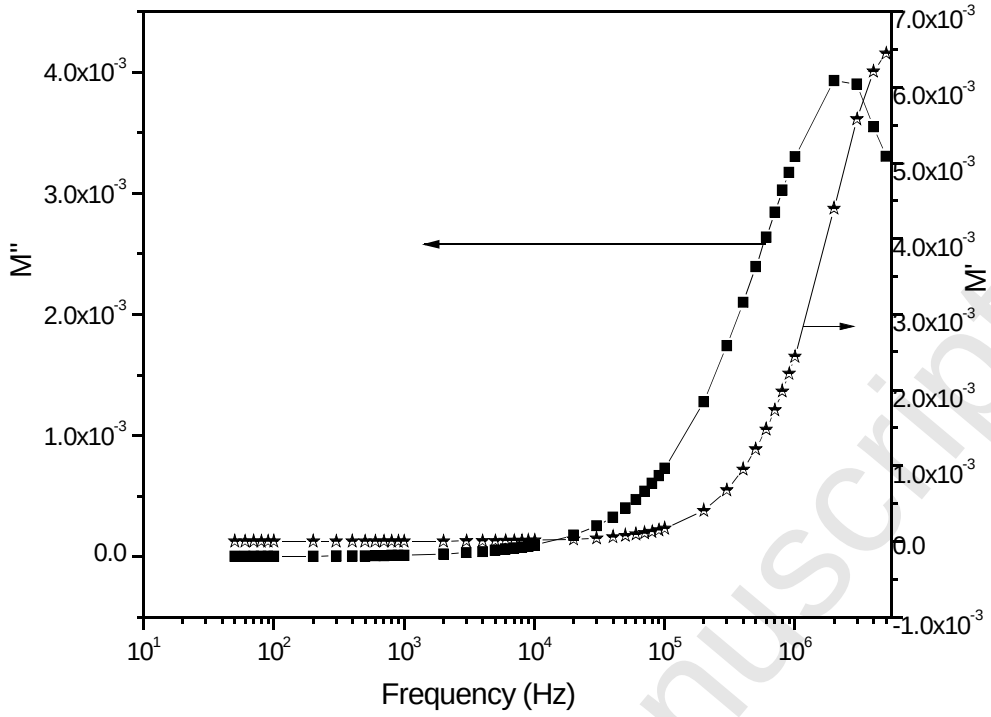

Figure 11 M' versus and M'' versus frequency for Pr doped $CaSiO_3$.

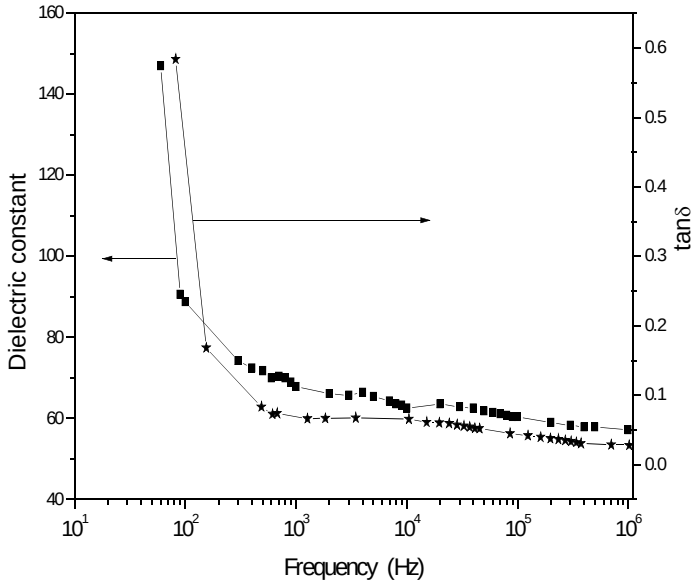

Figure 1 Dielectric constant and tanδ versus frequency for undoped $CaSiO_3$.

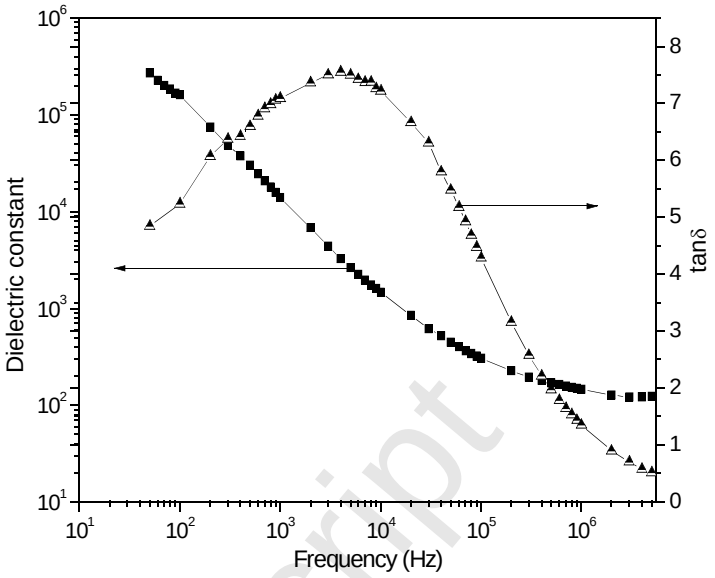

Figure 2 Dielectric constant and tanδ versus frequency . for Pr doped$CaSiO_3$

Graphical abstract:

Figures 1 and 2 show the graphs of dielectric constant and tanδ versus frequency for undoped and Pr doped $CaSiO_3$ respectively. Here we can observe normal dielectric properties for undoped $CaSiO_3$, where as an unusual effect in dielectric properties for Pr doped $CaSiO_3$.We have observed a colossal value for dielectric constant and a looss peak at resonant frequency for Pr doped $CaSiO_3$.

Highlights:

- $CaSiO3:Pr^{3+}$ was prepared by facile low temperature solution combustion method.
- The crystalline phase of the product is obtained by adopting sintering method.
- Samples prepared at $500\ ^0$ C and calcined at $900\ ^0$ C for 3 hours showed β- phase.
- The Pr^{3+} doped $CaSiO_3$ shows "unusual results".
- The electrical microstructure has been accepted to be of internal barrier layer capacitor.